A Switched Systems Framework for Path Following With Intermittent State Feedback

Hsi-Yuan Chen, Zachary I. Bell, Patryk Deptula, and Warren E. Dixon

***Abstract*—In many applications, autonomous agents are tasked with operating in regions where state feedback is unavailable. Inspired by such applications, a novel switched systems-based framework is developed for uncertain nonlinear systems subjected to temporary loss of state feedback. The framework developed in this letter facilitates the use of a predictor when state estimates are not available, and the use of an observer or a reset map when feedback becomes available. Maximum and minimum dwell-time conditions are derived via a Lyapunov-based switched systems analysis to ensure stability for the overall switched system. An approach for designing a novel auxiliary trajectory is provided to guide the agent in and out of the feedback denied region while adhering to dwell-time conditions. Experimental results are presented to demonstrate the performance of an example controller with an example predictor and observer or reset map using a quadcopter.**

***Index Terms*—Intermittent state feedback, switched systems framework, dwell-time conditions.**

I. Introduction

IN MANY scenarios, factors such as task definition, operating environment, or sensor modality can result in temporary loss of feedback for autonomous agents (e.g., communication may be limited or feedback may be provided by sensors such as cameras which are limited by sensing distance and field-of-view (FOV) constraints, and are vulnerable to occlusions). Such factors have motivated the development of various path planning and control methods that seek uninterrupted feedback (see [1]–[9]), where the desired trajectory or behavior of such systems is inherently constrained. As illustrated in [10]–[12], systems with nonholonomic constraints may experience limited, sharp-angled or non-smooth trajectories to keep a navigational landmark in the FOV using a visual servoing approach. In lieu of constraining the system to ensure uninterrupted feedback, the framework in this letter allows intermittent loss of state feedback for systems tasked with following paths that lie completely outside of a feedback region. Some applications where this framework is useful include underwater operations that require vehicles to resurface to acquire GPS, navigation within urban canyons where GPS is occluded, and exploration of areas where absolute positioning systems have not been established.

Previous literature from multiple communities have investigated approaches to allow intermittent loss of state feedback. For systems that utilize feedback from an imaging sensor, results such as [13] and [14] demonstrated a daisy-chaining approach where new landmarks or image features are localized with respect to the world frame and are used to provide state estimates when previous landmarks or features leave the FOV. However, the accuracy of the state estimate degrades over time in the presence of measurement noise and disturbances in the dynamics. Similarly, conventional approaches to the simultaneous localization and mapping (SLAM) problem (see [15]–[17]) use relationships between features or landmarks in a feature-rich environment with sufficient measurements to estimate the state of a system. A well-known drawback with SLAM algorithms is the proneness to drift in estimates caused by the accumulation of measurement noise (see [18], [19]). Typically, global loop closure algorithms are adopted to compensate for the accumulated error, but such algorithms are generally computationally intensive and cannot be performed in real time. The framework developed in this letter compensates for the error accumulation from disturbances, and a set of stabilizing conditions are provided to ensure global loop closures are achieved with respect to known landmarks or maps within a bounded estimation error.

Stochastic approaches typically model the intermittent loss of measurement as a random process with a known probability (see [20], [21]). The typical control objective for such systems is asymptotic convergence of the expected value of the estimation error in a probabilistic sense.[1]

In the network control systems community, results such as [23]–[25] utilize models of the controlled systems to propagate state estimates when feedback is unavailable. Typically, a decision maker is utilized to determine when to broadcast sensor information (i.e., sensor information is available to the

Manuscript received March 15, 2018; revised May 14, 2018; accepted June 1, 2018. Date of publication June 14, 2018; date of current version July 6, 2018. This work was supported by AFOSR under Award FA9550-18-1-0109. Recommended by Senior Editor S. Tarbouriech. *(Corresponding author: Hsi-Yuan Chen.)*

The authors are with the Department of Mechanical and Aerospace Engineering, University of Florida, Gainesville, FL 32611-6250 USA (e-mail: hychen@ufl.edu; bellz121@ufl.edu; pdeptula@ufl.edu; wdixon@ufl.edu).

Digital Object Identifier 10.1109/LCSYS.2018.2847416

[1] Although the objective in this letter is to purposefully leave the feedback region intermittently, random loss of state feedback could also be considered when the agent is inside the feedback region, such as modeled in [22], where the behavior of the actual tracking and estimation errors are examined.

agent wherever the agent is, provided some decision maker indicates that the information should be broadcast). In this letter, the availability of sensor information is based on the region in which the actual states are located, which introduces a unique constraint of state-based feedback availability (i.e., even if a decision maker indicates that state information should be made available, the agent still has to leave its current objective to return to a region where it can obtain state information).

In comparison to previous approaches, the result in this letter examines the challenge of intermittent feedback and the challenge of navigating an agent to a feedback available region while guaranteeing stability of the actual tracking and estimation errors. Specifically, the approach in this letter leverages switched systems methods to develop stabilizing conditions for an agent that temporarily leaves a region where feedback is available. In general, the stability of a switched system is achieved by imposing switching conditions on the subsystems to enforce a decrease in the overall Lyapunov function across switching instants. For slow, time-based switches, the switching conditions typically manifest as (average) dwell-time conditions, specifying the duration for which each subsystem must remain active [26]. In [27], an average dwell-time condition for switched systems with linear time invariant (LTI) stable and unstable subsystems is developed. Similarly, dwell-time conditions for nonlinear switched systems with exponentially stable and unstable subsystems were investigated in [28]. However, [27] also indicated that dwell-time conditions typically require the stable subsystems to be activated longer than the unstable subsystems. In [22], a switched systems framework for an image-based observer is developed where image features are intermittently occluded or leave the sensor FOV. An average dwell-time condition is provided to guarantee the convergence of the estimation error.

The most similar result to this letter is in [29] and [30]. The objective in [29] is to regulate a nonholonomic vehicle to a set-point by intermittently viewing a landmark, and the objective in [30] is for a holonomic agent to follow a path that lies outside a feedback region. However, the developments in [29] and [30] are control designs where the analysis dictates specific feedback and adaptive update laws, which constrain the system design. Furthermore, both results use specific observers dictated by the analysis require a minimum dwell-time when state feedback is available.

A novelty of the approach in this letter is the relaxation of the necessity to alter existing controllers and associated stability analysis, while maximizing the amount of time the agent is allowed in the feedback-denied environment. Furthermore, the current result allows a reset map to be used with no minimum dwell-time condition. These contributions allow a wide class of controllers, observers, or predictors to be used, and allows the agent to spend more time following the path in the feedback denied region. Using Lyapunov-based stability methods, a framework is developed to allow state estimators and predictors to be used when state feedback is or is not available, respectively, and switched systems analysis determines the stabilizing dwell-time conditions based on a prescribed tolerance on the tracking error. According to the developed dwell-time conditions, an auxiliary trajectory is designed to guide the nonlinear dynamic system in and out of the feedback denied region so that the overall system remains stable. Two experiments using a quadcopter are provided to demonstrate the performance of the approach.

II. System Model

Consider a nonlinear dynamic system subjected to an exogenous disturbance as

$$\dot{x}(t) = f(x(t), t) + v(x(t), t) + d(t), \tag{1}$$

where $x(t)$, $\dot{x}(t) \in \mathbb{R}^n$ denote a generalized state and its time derivative, $f : \mathbb{R}^n \times \mathbb{R} \to \mathbb{R}^n$ denotes the locally Lipschitz dynamics, $v(x(t), t) \in \mathbb{R}^n$ is the control input, and $d(t) \in \mathbb{R}^n$ is a bounded exogenous disturbance, where $\|d(t)\| \leq \bar{d} \in \mathbb{R}_{>0}$ with $n \in \mathbb{N}$ and $t \in \mathbb{R}_{\geq 0}$.

III. State Estimation and Control Objective

The objective is to enable an agent to follow a desired path, denoted by x_d, that lies completely outside of a region where feedback is available. Specifically, a known feedback region is denoted by a compact set $\mathcal{F} \subset \mathbb{R}^n$, and the region outside of the feedback region, denoted by $\mathcal{F}^c$, is the compliment of $\mathcal{F}$. Feedback is available when $x(t) \in \mathcal{F}$ and unavailable when $x(t) \in \mathcal{F}^c$ with $x_d \subset \mathcal{F}^c$. Since $x(t)$ is required to leave $\mathcal{F}$ to follow x_d, a state estimate $\hat{x}(t) \in \mathbb{R}^n$ is utilized to provide an estimate of $x(t)$. However, since open-loop estimators for unstable systems may diverge, the agent must occasionally return to the feedback region $\mathcal{F}$ to ensure the estimation error remains bounded. Since the agent is required to intermittently depart from following x_d to obtain feedback, a novel auxiliary trajectory, denoted by $x_\sigma(t) \in \mathbb{R}^n$, is developed to guide the agent between $\mathcal{F}$ and x_d. The design of $x_\sigma(t)$ is motivated by the desire to maximize the time $x(t)$ follows x_d, while adhering to subsequently developed dwell-time conditions. Given these objectives, three error systems are defined as

$$e(t) \triangleq x(t) - x_\sigma(t), \tag{2}$$

$$\hat{e}(t) \triangleq \hat{x}(t) - x_\sigma(t), \tag{3}$$

$$\tilde{e}(t) \triangleq x(t) - \hat{x}(t), \tag{4}$$

where $e(t)$ is the actual tracking error, $\hat{e}(t)$ is the estimate tracking error, and $\tilde{e}(t)$ is the state estimation error. When $x(t) \in \mathcal{F}$, the objective is to regulate all three error systems. When $x(t) \in \mathcal{F}^c$, state feedback is no longer available, and the objective is to regulate $\hat{e}(t)$; however, $\tilde{e}(t)$ may become unstable due to the lack of state feedback, and therefore, $e(t)$ may become unstable. As a result of potential instabilities when $x(t) \in \mathcal{F}^c$, another challenge in this letter is to ensure $e(t)$ does not grow beyond an application-based, desired bound while simultaneously maximizing the time $x(t) \in \mathcal{F}^c$ where $x(t)$ follows x_d. To facilitate the subsequent development, let $p \in \mathcal{P} \triangleq \{a, u\}$, where a is an index for the subsystem with available state feedback, and u is an index for the subsystem without state feedback.

Assumption 1: The system is initialized in a feedback region (i.e., $x(0) \in \mathcal{F}$).

IV. Stability Analysis

To illustrate framework development, consider any design of nonlinear controllers, observers (when $p = a$) and predictors (when $p = u$) that yield a family of closed-loop error dynamics of the forms

$$\dot{e}(t) = \begin{cases} g_{e,p}(v(x,t),t), & p = a, \\ g_{e,p}\big(v(\hat{x},t),t\big), & p = u, \end{cases} \tag{5}$$

$$\dot{\hat{e}}(t) = \begin{cases} g_{\hat{e},p}(v(x,t),t), & p = a, \\ g_{\hat{e},p}\big(v(\hat{x},t),t\big), & p = u, \end{cases} \tag{6}$$

$$\dot{\tilde{e}}(t) = g_{\tilde{e},p}\big(x,\hat{x},t\big), \ \ \forall p, \tag{7}$$

where $g_{e,p},\ g_{\hat{e},p} : \mathbb{R}^n \times [0,\infty) \to \mathbb{R}^n$ are nonlinear functions that depend on the controller, $g_{\tilde{e},p} : \mathbb{R}^n \times \mathbb{R}^n \times [0,\infty) \to \mathbb{R}^n$ is a nonlinear function that depends on the observer and predictor, and satisfy the following assumption.

Assumption 2: The origins of the error systems $e(t) = \tilde{e}(t) = 0$ is uniformly exponentially stable when $p = a$, and the origin of the error system $\hat{e}(t) = 0$ is uniformly exponentially stable when $p = u$. Furthermore, there exist three first-order differentiable, positive-definite candidate Lyapunov-like functions $V_e(e(t)),\ V_{\hat{e}}(\hat{e}(t)),\ V_{\tilde{e}}(\tilde{e}(t)) : \mathbb{R}^n \to \mathbb{R}$ such that

$$\dot{V}_e(e(t)) \le -2\lambda_s V_e(e(t)), \ \ p = a, \tag{8}$$

$$\dot{V}_{\hat{e}}(\hat{e}(t)) \le -2\lambda_s V_{\hat{e}}(\hat{e}(t)), \ \ p = u, \tag{9}$$

$$\dot{V}_{\tilde{e}}(\tilde{e}(t)) \le \begin{cases} -2\lambda_{\tilde{e}} V_{\tilde{e}}(\tilde{e}(t)), & p = a, \\ 2\lambda_u V_{\tilde{e}}(\tilde{e}(t)) + \delta, & p = u, \end{cases} \tag{10}$$

where $\lambda_s,\ \lambda_{\tilde{e}},\ \lambda_u,\ \delta \in \mathbb{R}_{>0}$ are known, positive constants.

To further facilitate the analysis for the switched system, let the time of the i^{th} instance when $x(t)$ transitions from $\mathcal{F}^c$ to $\mathcal{F}$ and from $\mathcal{F}^c$ to $\mathcal{F}$ be denoted by $t_i^a \in \mathbb{R}_{\ge 0}$ and $t_i^u \in \mathbb{R}_{>0}$, respectively, for $i \in \mathbb{N}$. Based on the switching instants, dwell-time of the i^{th} activation of the subsystems a and u are defined as $\Delta t_i^a \triangleq t_i^u - t_i^a \in \mathbb{R}_{>0}$ and $\Delta t_i^u \triangleq t_{i+1}^a - t_i^u \in \mathbb{R}_{>0}$, respectively. To ensure the tracking error is bounded, a minimum threshold $\hat{e}_T \in \mathbb{R}_{>0}$ on $\|\hat{e}(t)\|$ and a desired maximum bound $e_M \ge 2\hat{e}_T$ on $\|e(t)\|$ may be imposed such that $V_e(e(t_i^a)) \le V_M$ and $V_{\hat{e}}(\hat{e}(t_i^u)) \le V_T$, where $V_M,\ V_T \in \mathbb{R}_{>0}$ are the respective maximum bound and minimum threshold. Since $\|\hat{e}(t_i^u)\| \le \|e(t_i^u)\| + \|\tilde{e}(t_i^u)\| \le \hat{e}_T$, it follows that $\|e(t_i^u)\| \le \hat{e}_T$ and $\|\tilde{e}(t_i^u)\| \le \hat{e}_T$; furthermore, since $\|e(t_i^a)\| \le \|\hat{e}(t_i^a)\| + \|\tilde{e}(t_i^a)\| \le e_M$, it follows that $\|\hat{e}(t_i^a)\| \le e_M$ and $\|\tilde{e}(t_i^a)\| \le e_M$. The selection on e_M is also dictated by the size of $\mathcal{F}$, where the compact ball of radius e_M must be less than or equal to the inscribed ball of $\mathcal{F}$ in $\mathbb{R}^n$.

Theorem 1: The trajectories of the switched systems generated by the family of subsystems described by (5) - (7), and a piecewise constant, right-continuous switching signal $\sigma : [0,\infty) \to p \in \{a,u\}$ are globally uniformly ultimately bounded provided the switching signal satisfies the minimum feedback availability dwell-time condition

$$\Delta t_i^a \ge \frac{-1}{\min(\lambda_s,\lambda_{\tilde{e}})} \ln\left(\min\left(\frac{\hat{e}_T}{\big(\|e(t_i^a)\| + \|\tilde{e}(t_i^a)\|\big)}, 1\right)\right), \tag{11}$$

and the maximum loss of feedback dwell-time condition

$$\Delta t_i^u \le \ln(X_{min}), \tag{12}$$

where X_{min} is a subsequently defined positive constant.

Proof: While $p = a$, it can be shown from (8) - (10) that $e(t)$ and $\tilde{e}(t)$ are globally exponentially stable with the bounds

$$\|e(t)\| \le \|e(t_i^a)\| e^{-\lambda_s \Delta t_i^a}, \tag{13}$$

$$\|\tilde{e}(t)\| \le \|\tilde{e}(t_i^a)\| e^{-\lambda_{\tilde{e}} \Delta t_i^a}. \tag{14}$$

Utilizing the relationship $\hat{e}(t) = e(t) - \tilde{e}(t) \implies \|\hat{e}(t)\| \le \|e(t)\| + \|\tilde{e}(t)\| \implies \|\hat{e}(t)\| \le \|e(t_i^a)\| e^{-\lambda_s \Delta t_i^a} + \|\tilde{e}(t_i^a)\| e^{-\lambda_{\tilde{e}} \Delta t_i^a} \le \|e(t_i^a)\| e^{-\min(\lambda_s,\lambda_{\tilde{e}})\Delta t_i^a} + \|\tilde{e}(t_i^a)\| e^{-\min(\lambda_s,\lambda_{\tilde{e}})\Delta t_i^a} \implies \|\hat{e}(t)\| \le (\|e(t_i^a)\| + \|\tilde{e}(t_i^a)\|) e^{-\min(\lambda_s,\lambda_{\tilde{e}})\Delta t_i^a}$. Based on the convergence rate of $\|\hat{e}(t)\|$, the minimum dwell-time condition can be derived as $\|\hat{e}(t_i^u)\| \le \hat{e}_T \implies (\|e(t_i^a)\| + \|\tilde{e}(t_i^a)\|) e^{-\min(\lambda_s,\lambda_{\tilde{e}})\Delta t_i^a} \le \hat{e}_T$, and therefore the minimum dwell-time condition in (11) can be obtained by solving the inequality.

While $p = u$, it can be shown from (8) - (10) that the evolution of $\hat{e}(t)$ and $\tilde{e}(t)$ are bounded by

$$\|\hat{e}(t)\| \le \|\hat{e}(t_i^u)\| e^{-\lambda_s \Delta t_i^u}, \tag{15}$$

$$\|\tilde{e}(t)\| \le \sqrt{\|\tilde{e}(t_i^u)\|^2 e^{2\lambda_u \Delta t_i^u} - \frac{\delta}{2\lambda_u}\Big(1 - e^{2\lambda_u \Delta t_i^u}\Big)}. \tag{16}$$

Utilizing the relationship $e(t) = \hat{e} + \tilde{e}(t)$, $\|e(t)\| \le \|\hat{e}(t)\| + \|\tilde{e}(t)\| \implies \|e(t)\| \le \|\hat{e}(t_i^u)\| e^{-\lambda_s \Delta t_i^u} + \sqrt{\|\tilde{e}(t_i^u)\|^2 e^{2\lambda_u \Delta t_i^u} - \frac{\delta}{\lambda_u}(1 - e^{2\lambda_u \Delta t_i^u})}$. Substituting in the desired error bound of $e(t_{i+1}^a) \le e_M$ and performing algebraic manipulations yields $\|\hat{e}(t_i^u)\|^2 X^{-2\lambda_s} - 2e_M \|\hat{e}(t_i^u)\| X^{-\lambda_s} - \|\tilde{e}(t_i^u)\|^2 X^{2\lambda_u} - \frac{\delta}{2\lambda_u} X^{2\lambda_u} + e_M^2 + \frac{\delta}{2\lambda_u} \ge 0$, where $X = e^{\Delta t_i^u}$. Numerical solutions for X can be computed, and by taking the natural logarithm on the minimum positive, real solution $X_{min} \in \mathbb{R}_{\ge 1}$, the maximum dwell-time condition can be derived. ∎

Remark 1: A more conservative bound on the maximum dwell-time condition in (12) for continuous state estimates can be derived by upper bounding $\|\hat{e}(t)\|$ by $\|\hat{e}(t)\| \le \|\hat{e}(t_i^u)\| e^{-\lambda_s \Delta t_i^u} \le \|\hat{e}(t_i^u)\|$ to yield $\Delta t_i^u \le \frac{1}{2\lambda_u} \ln\left(\frac{(e_M - \|\hat{e}(t_i^u)\|)^2 + \frac{\delta}{2\lambda_u}}{\|\tilde{e}(t_i^u)\|^2 + \frac{\delta}{2\lambda_u}}\right)$.

A. Utilizing Reset Maps

The result in Theorem 1 relies on an observer to provide state estimates when $x(t) \in \mathcal{F}$, which results in a minimum dwell-time condition. However, the minimum dwell-time condition can be eliminated by using reset maps. Specifically, it is possible to exploit reset maps to reset $x_{\sigma,i}$ to a new path $x_{\sigma,i+1}$ and $\hat{x}(t)$ to coincide $x(t)$ at t_i^a, i.e., upon every instance of re-entry to $\mathcal{F}$. However, imposing reset maps on x_σ and $\hat{x}(t)$ introduces a discontinuity in the error dynamics; hence, a switched hybrid system analysis is required. To facilitate the development, let $E \subset \mathscr{P} \times \mathscr{P}$ represent a one-way transition from $p = u$ to $p = a$. Let the reset maps for x_σ and $\hat{x}(t)$ be denoted as $\phi_\sigma : E \times x_{\sigma,i} \to \mathbb{R}^n$ and $\hat{\phi} : E \times \mathbb{R}^n \to \mathbb{R}^n$, respectively, and be designed as $\phi_\sigma(E, x_{\sigma,i}(t)) \triangleq x_{\sigma,i+1}$ and $\hat{\phi}(E, \hat{x}(t)) \triangleq x(t)$.

When x_{σ_i} and $\hat{x}(t)$ are reset at t_i^a, $e(t) = \tilde{e}(t) = 0$, and hence, $\hat{e}(t) = 0$. It can be shown that the switches satisfy the *sequence non-increasing condition* described

in [31], such that $V_e(e(t_i^{a-})) \geq V_e(e(t_i^a))$, $V_{\hat{e}}(\hat{e}(t_i^{a-})) \geq V_{\hat{e}}(\hat{e}(t_i^a))$ and $V_{\tilde{e}}(\tilde{e}(t_i^{a-})) \geq V_{\tilde{e}}(\tilde{e}(t_i^a))$, where $t_i^{a-} \triangleq \lim t \to t_i^a$ from the left. Following a similar proof for Theorem 1, with the exception that $e(t) = \hat{e}(t) = \tilde{e}(t) = 0$ when $p = a$, the same stability conditions can be obtained. Since $e_T > e(t) = 0$, the minimum tracking error condition is automatically and instantaneously satisfied, indicating that $x(t)$ may leave $\mathcal{F}$ immediately upon entry, i.e., $\Delta t_i^a \geq 0$. Utilizing $\|\hat{e}(t_i^u)\| = 0$, the maximum dwell-time condition can then be solved analytically as $\|\tilde{e}(t_i^u)\|^2 e^{2\lambda_u \Delta t_i^u} - \frac{\delta}{2\lambda_u} e^{2\lambda_u \Delta t_i^u} + e_M^2 + \frac{\delta}{2\lambda_u} \geq 0$, and therefore $\Delta t_i^u \leq \frac{1}{2\lambda_u} \ln\left(\frac{e_M^2 + \frac{\delta}{2\lambda_u}}{\|\tilde{e}(t_i^u)\|^2 + \frac{\delta}{2\lambda_u}}\right)$.

V. Auxiliary Trajectory Design

Since x_d denotes a path that lies outside the feedback region, i.e., $x_d \subset \mathcal{F}^c$, $x(t)$ must leave $\mathcal{F}$ while following x_d, resulting in the loss of feedback. Therefore, an auxiliary trajectory $x_\sigma(t)$ is designed for the agent to track so that $x(t)$ follows x_d to the extent possible given the dwell-time conditions in (11) and (12). To facilitate the development of $x_\sigma(t)$, let the closest orthogonal projection of $x_\sigma(t)$ on the boundary of $\mathcal{F}$ be denoted as $x_b(t) \in \mathbb{R}^n$.

While $x(t) \in \mathcal{F}^c$, $\|e(t)\|$ can be upper bounded by e_M when the maximum dwell-time is reached, implying that there exist a compact set $\mathcal{B} = \{y \in \mathbb{R}^n | \|y - x_\sigma(t)\| \leq e_M\}$ such that $x(t) \in \mathcal{B}$, $\forall t$. To compensate for the potential accumulation of error, $x_\sigma(t)$ must penetrate a sufficient distance into $\mathcal{F}$, motivating the design of a cushion state $x_\epsilon(t) \in \mathbb{R}^n$ as

$$x_\epsilon(t) \triangleq x_b(t) + \Phi(t), \tag{17}$$

where $\Phi(t) \in \mathbb{R}^n$, such that $\|\Phi(t)\| \geq e_M$ and there exist a compact set $\mathcal{A} = \{y \in \mathbb{R}^n | \|y - x_\epsilon(t)\| \leq \|\Phi(t)\|\}$ such that $\mathcal{A}$ is less than or equal to the inscribed ball of $\mathcal{F}$ in $\mathbb{R}^n$. Therefore, the requirement of $x(t) \in \mathcal{B} \subseteq \mathcal{A} \subseteq \mathcal{F}$ can be satisfied if $x_\sigma(t)$ coincides with $x_\epsilon(t)$ when the maximum dwell-time is reached.

VI. Design Example

To illustrate the developed framework, consider an example controller designed as

$$v\big(x_p(t), t\big) \triangleq \dot{x}_\sigma(t) - \left(k + \frac{\bar{d}^2}{\varepsilon} I_n\right)\big(x_p(t) - x_\sigma(t)\big) - f\big(x_p(t), t\big), \tag{18}$$

where $x_p(t) = x(t)$ when $p = a$ and $x_p(t) = \hat{x}(t)$ when $p = u$, $k \in \mathbb{R}^{n \times n}$ is a constant, positive-definite gain matrix, I_n is a $n \times n$ identity matrix, and $\varepsilon \in \mathbb{R}_{>0}$ a design parameter. In (18), the design structure remains the same for all p, where only the input signal switches between using $x(t)$ or $\hat{x}(t)$.

Examples of the state estimate update laws for the observer and predictor are given as

$$\dot{\hat{x}}(t) \triangleq \begin{cases} f(\hat{x}(t), t) + v(x(t), t) + v_r(\tilde{e}(t)), & p = a, \\ f(\hat{x}(t), t) + v(\hat{x}(t), t), & p = u, \end{cases} \tag{19}$$

where $v_r(\tilde{e}(t)) \in \mathbb{R}^n$ contains a high-frequency sliding-mode term to compensate for disturbances and is designed as

$$v_r(\tilde{e}(t)) \triangleq k_{\tilde{e}} \tilde{e}(t) + \bar{d} sgn(\tilde{e}(t)), \tag{20}$$

where $k_{\tilde{e}} \in \mathbb{R}^{n \times n}$ is a constant, positive-definite gain matrix. Unlike the development in [29] and [30], the controller does not require canceling terms since the controller receives $x(t)$ as feedback when $p = a$ and the robustifying term is not added to the predictor when $p = u$. Additionally, the controller and observer designs are decoupled and can be designed independently under the framework developed in Section IV.

After taking the time derivative of (2) - (4), substituting in (1) and (18) - (20) and selecting the candidate Lyapunov-like functions as $V_e(e(t)) \triangleq \frac{1}{2} e^T(t) e(t)$, $V_{\hat{e}}(\hat{e}(t)) \triangleq \frac{1}{2} \hat{e}^T(t) \hat{e}(t)$ and $V_{\tilde{e}}(\tilde{e}(t)) \triangleq \frac{1}{2} \tilde{e}^T(t) \tilde{e}(t)$, the known, positive constants in (8) -(10) are determined as $\lambda_s = \underline{k}$, $\lambda_{\tilde{e}} = \underline{k}_{\tilde{e}} - c$, $\lambda_u = c + \frac{1}{2}$, $\lambda_s > 0$, and $\delta = \frac{1}{2}\bar{d}^2$, where $\underline{k} > 0$ and $\underline{k}_{\tilde{e}} > c$ are the minimum eigenvalues of k and $k_{\tilde{e}}$, respectively, and $c \in \mathbb{R}_{>0}$ is a Lipschitz constant. The tracking error $\|e(t)\|$ is shown to exponentially converge $\forall \|e(t)\| > \sqrt{\frac{\varepsilon}{4\lambda_s}}$. Hence, the dwell-time conditions can be derived accordingly, where $\hat{e}_T > \sqrt{\frac{\varepsilon}{4\lambda_s}}$.

To illustrate the design of the auxiliary trajectory, an example of $x_\sigma(t)$ using an observer is given as

$$x_{\sigma,i}(t) \triangleq \begin{cases} \rho_i^a x_\epsilon(t) + \big(1 - \rho_i^a\big) x_b(t), & t_i^a \leq t < t_i^u, \\ \rho_i^{u1} x_b(t) + \big(1 - \rho_i^{u1}\big) g(x_d, t), & t_i^u \leq t < t_i^{u1}, \\ g(x_d, t), & t_i^{u1} \leq t < t_i^{u2}, \\ \rho_i^{u3} g(x_d, t) + \big(1 - \rho_i^{u3}\big) x_\epsilon(t), & t_i^{u2} \leq t < t_i^{u3}, \end{cases} \tag{21}$$

where $g : x_d \times \mathbb{R} \to \mathbb{R}^n$ maps t to the desired state in x_d, ρ_i^a, ρ_i^{u1}, ρ_i^{u2} and ρ_i^{u3} are time-based ratios designed as $\rho_i^a \triangleq \frac{t - t_i^a}{\Delta t_i^a}$ and $\rho_i^{u(j+1)} \triangleq \frac{t - (t_i^u + \sum_{k=0}^{j} p_k \Delta t_i^u)}{p_{j+1} \Delta t_i^u}$, $j \in \{0, 1, 2\}$, the weights used to partition the maximum dwell-time are denoted by $p_k \in [0, 1)$, and the corresponding partitions are denoted by $t_i^{u(j+1)}$. In addition, t_i^{u3} coincides with t_{i+1}^a, and Δt_i^a must be arbitrarily lower bounded above zero to avoid a singularity in ρ_i^a.

If a reset map is used instead of the observer, the auxiliary trajectory can be designed as

$$x_{\sigma,i}(t) \triangleq \begin{cases} \rho_i^{u1} x(t) + \big(1 - \rho_i^{u1}\big) g(x_d, t), & t_i^u \leq t < t_i^{u1}, \\ g(x_d, t), & t_i^{u1} \leq t < t_i^{u2}, \\ \rho_i^{u3} g(x_d, t) + \big(1 - \rho_i^{u3}\big) x_\epsilon(t), & t_i^{u2} \leq t < t_i^{u3}. \end{cases} \tag{22}$$

VII. Experimental Results

Two experiments are conducted to demonstrate the ability of an unmanned air vehicle to follow a path that lies outside a feedback region. Specifically, the objective is to examine the boundedness of the tracking error $e(t)$, and therefore stability of the system, throughout multiple revisits to the feedback region based on the dwell-time constraints established in Theorem 1. Both experiments use the example controller and predictor in (18) and (19), respectively. One experiment uses the observer in (19) and (20) with $x_\sigma(t)$ given in (21). The other experiment uses a reset map with $x_\sigma(t)$ given in (22).

For both experiments, a Parrot Bebop 2.0 quadcopter is used as the unmanned air vehicle. The quadcopter is equipped with a magnetometer, a 3-axis gyroscope, a 3-axis accelerometer, and an optical-flow sensor. Estimates of the linear and angular velocities of the quadcopter are provided by the on-board

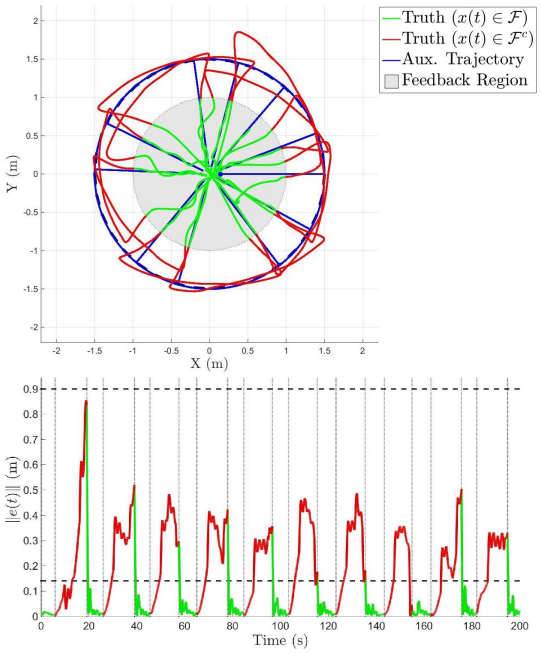

Fig. 1. Overall path following result and the evolution of $\|e(t)\|$ for continuous state estimates. The tracking error is regulated below $\hat{e}_T$ (bottom dotted line) before leaving $\mathcal{F}$ and remains under e_M (top dotted line) for all times when outside of $\mathcal{F}$. The vertical lines denote the instants when $x(t)$ enters and leaves $\mathcal{F}$.

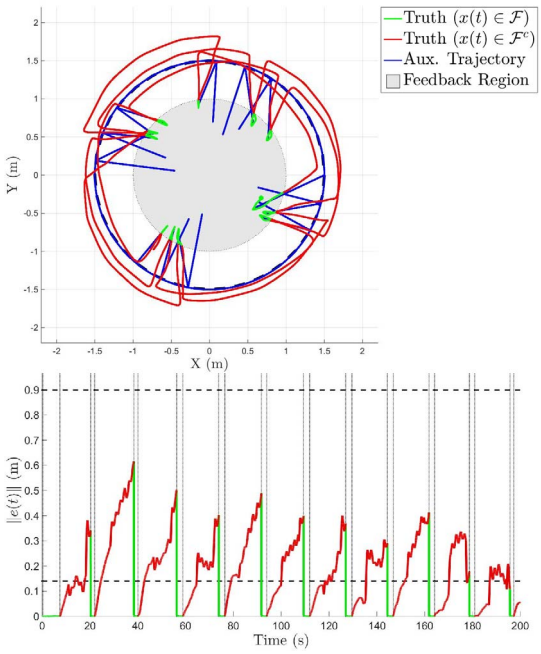

Fig. 2. Overall path following result and the evolution of $\|e(t)\|$ for discrete state estimates using a reset map. The tracking error is regulated below $\hat{e}_T$ (bottom dotted line) before leaving $\mathcal{F}$ and remains under e_M (top dotted line) for all times when outside of $\mathcal{F}$. The vertical lines denote the instants when $x(t)$ enters and leaves $\mathcal{F}$.

sensors at a rate of 5Hz. A ground station generates velocity commands using the Robotic Operating System (ROS) Kinetic framework in Ubuntu 16.04. The *bebop_autonomy* package developed by [32] is used to broadcast velocity commands to the quadcopter through a WiFi channel of 5GHz.

To simulate a feedback signal and record the ground truth pose of the quadcopter, a NaturalPoint, Inc. OptiTrack motion capture system is used. The feedback available region $\mathcal{F}$ is defined as a region inside a 1-meter circle, and x_d is a 1.5-meter circle with the same origin as $\mathcal{F}$. Pose information obtained from the motion capture system is used as feedback only when the quadcopter is inside $\mathcal{F}$. Even though the OptiTrack system continues to record pose information when the quadcopter is outside the feedback region, the information is only used as ground truth for comparison purposes. For both experiments, on-board velocity measurements are utilized to match the velocity commands generated by the ground station.

Simplified dynamics of the quadcopter are represented by $\dot{x}(t) = u(t) + d(t)$, where $x(t)$ is the composite vector of the Euclidean coordinates of the quadcopter with respect to the inertial frame. For both experiments, the upper bound of the disturbance is assumed to be $\bar{d} = 0.05$, and the controller and update law are designed as described in Section VI, where $f(x,t) = f(\hat{x},t) = \begin{bmatrix} 0 & 0 & 0 \end{bmatrix}^T$, $k = 0.4I_3$, $k_{\tilde{e}} = 4I_3$, and $\varepsilon = 0.02$.

The auxiliary trajectory $x_\sigma(t)$ is designed to follow x_d with an angular velocity of $\frac{\pi}{15}$ radians per second during $t_i^{u1} \leq t < t_i^{u2}$, and the partitions for the maximum dwell-time are selected as $p_0 = 0$, $p_1 = 0.4$, $p_2 = 0.3$, $p_3 = 0.3$. The desired error bound and threshold are selected as $e_M = 0.9$ meters and $\hat{e}_T = 0.14$ meters. Since single integrator dynamics are used for the quadcopter, the Appendix provides a less conservative minimum dwell-time condition that is implemented for both experiments.

Figures 1 and 2 illustrate the experimental results using the observer and reset map, respectively. When using the observer, the quadcopter is allowed to remain in $\mathcal{F}^c$ for 16.10 seconds and is required to remain in $\mathcal{F}$ for 3.59 seconds on average. When using the reset map, the quadcopter is allowed 18.00 seconds in $\mathcal{F}^c$ and no minimum dwell-times are required. In both experiments, the tracking error converges exponentially when $x(t) \in \mathcal{F}$ and exhibits growth when $x(t) \in \mathcal{F}^c$, reflecting the analysis in Section IV. The growth of $\|e(t)\|$ can be attributed to the open-loop tracking performance, and various techniques (e.g., the use of inertial measurement units or visual odometry) can be applied to minimize the open-loop tracking error when $x(t) \in \mathcal{F}^c$. The goal for both experiments is to demonstrate the developed switching framework that allows the quadcopter to compensate for the lack of feedback and achieve timely loop-closures such that the tracking error growth stays bounded. As shown in Figures 1 and 2, $\|e(t)\|$ is upper bounded by e_M, and converges to below $\hat{e}_T$ before leaving $\mathcal{F}$. Therefore, these experiments demonstrate that the switching signal $\sigma(t)$ generated by $x_\sigma(t)$ satisfies the dwell-time conditions developed in Section IV and stabilizes the overall system.

VIII. Conclusion

A novel method that establishes a switched systems framework for path following under an intermittent state feedback constraint is presented. Specifically, the presented method

relieves the requirement of uninterrupted state feedback, and allows the system to dwell in a feedback-denied region for periods of time. In addition, applicable controllers and observers from existing literature can be directly implemented without altering the design structure, stability analysis, or gain selection. Maximum and minimum dwell-time conditions are developed via a Lyapunov-based, switched systems analysis to guarantee stability of the overall system. Alternatively, the analysis indicates that reset maps can also be utilized to eliminate the requirement of minimum dwell-time conditions. an auxiliary trajectory is designed based on the dwell-time conditions to regulate the states into the feedback region before the tracking error exceeds a defined threshold. Two experiments were performed to illustrate the control development and trajectory design with and without using reset maps. The results indicate that using reset maps allows the agent to spend more time in the feedback denied region. Future research will focus on the development of optimal path planning methods. Additional research will also target cases where the feedback region is time-varying or unknown.

APPENDIX

With single integrator dynamics, the estimation error dynamics are upper bounded by $\dot{\tilde{e}}(t) \leq \bar{d}$ when $p = u$, and therefore $\tilde{e}(t)$ exhibits a linear growth that can be bounded by $\|\tilde{e}(t)\| \leq \|\tilde{e}(t_i^u)\| + \bar{d}(\Delta t_i^u)$. Following the development in Section IV, the maximum dwell-time can be derived by solving the inequality as $\|\hat{e}(t_i^u)\|e^{-\lambda_s \Delta t_i^u} + \|\tilde{e}(t_i^u)\| + \bar{d}(\Delta t_i^u) \leq e_M$, $\|\hat{e}(t_i^u)\| + \|\tilde{e}(t_i^u)\| + \bar{d}(\Delta t_i^u) \leq e_M$, and therefore $\Delta t_i^u \leq \frac{e_M - \|\hat{e}(t_i^u)\| - \|\tilde{e}(t_i^u)\|}{\bar{d}}$.

REFERENCES

[1] S. Hutchinson, G. D. Hager, and P. I. Corke, "A tutorial on visual servo control," *IEEE Trans. Robot. Autom.*, vol. 12, no. 5, pp. 651–670, Oct. 1996.

[2] N. R. Gans, G. Hu, K. Nagarajan, and W. E. Dixon, "Keeping multiple moving targets in the field of view of a mobile camera," *IEEE Trans. Robot.*, vol. 27, no. 4, pp. 822–828, Aug. 2011. [Online]. Available: http://ncr.mae.ufl.edu/papers/TRO11.pdf

[3] G. Hu, N. Gans, and W. E. Dixon, "Quaternion-based visual servo control in the presence of camera calibration error," *Int. J. Robust Nonlin. Control*, vol. 20, no. 5, pp. 489–503, 2010. [Online]. Available: http://ncr.mae.ufl.edu/papers/RNC10.pdf

[4] G. Hu, N. Gans, N. Fitz-Coy, and W. E. Dixon, "Adaptive homography-based visual servo tracking control via a quaternion formulation," *IEEE Trans. Control Syst. Technol.*, vol. 18, no. 1, pp. 128–135, Jan. 2010. [Online]. Available: http://ncr.mae.ufl.edu/papers/CST10.pdf

[5] G. Hu *et al.*, "Homography-based visual servo control with imperfect camera calibration," *IEEE Trans. Autom. Control*, vol. 54, no. 6, pp. 1318–1324, Jun. 2009. [Online]. Available: http://ncr.mae.ufl.edu/papers/tac09.pdf

[6] J. Chen, D. M. Dawson, W. E. Dixon, and V. Chitrakaran, "Navigation function-based visual servo control," *Automatica*, vol. 43, no. 7, pp. 1165–1177, 2007. [Online]. Available: http://ncr.mae.ufl.edu/papers/auto07.pdf

[7] G. Palmieri, M. Palpacelli, M. Battistelli, and M. Callegari, "A comparison between position-based and image-based dynamic visual servoings in the control of a translating parallel manipulator," *J. Robot.*, vol. 2012, 2012, Art. no. 103954.

[8] N. R. Gans and S. A. Hutchinson, "Stable visual servoing through hybrid switched-system control," *IEEE Trans. Robot.*, vol. 23, no. 3, pp. 530–540, Jun. 2007.

[9] G. Chesi and A. Vicino, "Visual servoing for large camera displacements," *IEEE Trans. Robot.*, vol. 20, no. 4, pp. 724–735, Aug. 2004.

[10] N. R. Gans and S. A. Hutchinson, "A stable vision-based control scheme for nonholonomic vehicles to keep a landmark in the field of view," in *Proc. IEEE Int. Conf. Robot. Autom.*, Rome, Italy, Apr. 2007, pp. 2196–2201.

[11] G. L. Mariottini, G. Oriolo, and D. Prattichizzo, "Image-based visual servoing for nonholonomic mobile robots using epipolar geometry," *IEEE Trans. Robot.*, vol. 23, no. 1, pp. 87–100, Feb. 2007.

[12] G. Lopez-Nicolas *et al.*, "Homography-based control scheme for mobile robots with nonholonomic and field-of-view constraints," *IEEE Trans. Syst., Man, Cybern. B, Cybern.*, vol. 40, no. 4, pp. 1115–1127, Aug. 2010.

[13] S. S. Mehta, T. Burks, and W. E. Dixon, "A theoretical model for vision-based localization of a wheeled mobile robot in greenhouse applications: A daisy chaining approach," *Comput. Electron. Agric.*, vol. 63, pp. 28–37, Aug. 2008.

[14] B. Jia and S. Liu, "Switched visual servo control of nonholonomic mobile robots with field-of-view constraints based on homography," *Control Theory Technol.*, vol. 13, no. 4, pp. 311–320, 2015.

[15] G. Klein and D. Murray, "Parallel tracking and mapping for small AR workspaces," in *Proc. IEEE ACM Int. Symp. Mixed Augmented Reality*, Nara, Japan, 2007, pp. 225–234.

[16] A. J. Davison, I. D. Reid, N. D. Molton, and O. Stasse, "MonoSLAM: Real-time single camera SLAM," *IEEE Trans. Pattern Anal. Mach. Intell.*, vol. 29, no. 6, pp. 1052–1067, Jun. 2007.

[17] D. Cremers, "Direct methods for 3D reconstruction and visual SLAM," in *Proc. IEEE IAPR Int. Conf. Mach. Vis. Appl.*, Nagoya, Japan, 2017, pp. 34–38.

[18] B. Williams *et al.*, "A comparison of loop closing techniques in monocular SLAM," *Robot. Auton. Syst.*, vol. 57, no. 12, pp. 1188–1197, 2009.

[19] C. Cadena *et al.*, "Past, present, and future of simultaneous localization and mapping: Toward the robust-perception age," *IEEE Trans. Robot.*, vol. 32, no. 6, pp. 1309–1332, Dec. 2016.

[20] S. Kluge, K. Reif, and M. Brokate, "Stochastic stability of the extended Kalman filter with intermittent observations," *IEEE Trans. Autom. Control*, vol. 55, no. 2, pp. 514–518, Feb. 2010.

[21] L. Li and Y. Xia, "Stochastic stability of the unscented Kalman filter with intermittent observations," *Automatica*, vol. 48, no. 5, pp. 978–981, 2012.

[22] A. Parikh, T.-H. Cheng, H.-Y. Chen, and W. E. Dixon, "A switched systems framework for guaranteed convergence of image-based observers with intermittent measurements," *IEEE Trans. Robot.*, vol. 33, no. 2, pp. 266–280, Apr. 2017.

[23] E. Garcia and P. J. Antsaklis, "Adaptive stabilization of model-based networked control systems," in *Proc. Amer. Control Conf.*, San Francisco, CA, USA, Jun./Jul. 2011, pp. 1094–1099.

[24] E. Garcia and P. J. Antsaklis, "Model-based event-triggered control for systems with quantization and time-varying network delays," *IEEE Trans. Autom. Control*, vol. 58, no. 2, pp. 422–434, Feb. 2013.

[25] M. J. McCourt, E. Garcia, and P. J. Antsaklis, "Model-based event-triggered control of nonlinear dissipative systems," in *Proc. Amer. Control Conf.*, Portland, OR, USA, Jun. 2014, pp. 5355–5360.

[26] D. Liberzon, *Switching in Systems and Control*. Boston, MA, USA: Birkhäuser, 2003.

[27] G. Zhai, B. Hu, K. Yasuda, and A. N. Michel, "Stability analysis of switched systems with stable and unstable subsystems: An average dwell time approach," *Int. J. Syst. Sci.*, vol. 32, no. 8, pp. 1055–1061, Nov. 2001.

[28] M. A. Müller and D. Liberzon, "Input/output-to-state stability and state-norm estimators for switched nonlinear systems," *Automatica*, vol. 48, no. 9, pp. 2029–2039, 2012.

[29] H.-Y. Chen, Z. I. Bell, R. Licitra, and W. E. Dixon, "A switched systems approach to vision-based tracking control of wheeled mobile robots," in *Proc. IEEE Conf. Decis. Control*, Melbourne, VIC, Australia, 2017, pp. 4902–4907.

[30] H.-Y. Chen, Z. I. Bell, P. Deptula, and W. E. Dixon, "A switched systems approach for path following with intermittent state feedback," *IEEE Trans. Robot.*, submitted for publication. [Online]. Available: https://arxiv.org/abs/1803.05584

[31] M. S. Branicky, "Multiple Lyapunov functions and other analysis tools for switched and hybrid systems," *IEEE Trans. Autom. Control*, vol. 43, no. 5, pp. 475–482, Apr. 1998.

[32] *bebop_Autonomy Library*. Accessed: Mar. 20, 2018. [Online]. Available: http://bebop-autonomy.readthedocs.io